Title
REACTIVE COLLISIONS IN CROSSED MOLECULAR BEAMS

Author
Herschbach, Dudley R.

Publication Date
1962-02-12

UCRL 10096

UNIVERSITY OF CALIFORNIA

Ernest O. Lawrence Radiation Laboratory

BERKELEY, CALIFORNIA

For Proceedings of Faraday Society Discussion on
"Inelastic Collisions of Atoms and Simple Molecules"
Cambridge University - April 10-12, 1962

UCRL-10096

UNIVERSITY OF CALIFORNIA

Lawrence Radiation Laboratory
Berkeley, California

Contract No. W-7405-eng-48

REACTIVE COLLISIONS IN CROSSED MOLECULAR BEAMS

Dudley R. Herschbach

February, 1962

Paper to be presented at the Faraday Society Discussion on
"Inelastic Collisions of Atoms and Simple Molecules,"
Cambridge University, April 10-12, 1962

UCRL-10096

REACTIVE COLLISIONS IN CROSSED MOLECULAR BEAMS*

By Dudley R. Herschbach

Department of Chemistry, University of
California, Berkeley, California

Abstract

The distribution of velocity vectors of reaction products is discussed, with emphasis on the restrictions imposed by the conservation laws. The recoil velocity which carries the products away from the center of mass shows how the energy of reaction is divided between internal excitation and translation. Similarly, the angular distributions, as viewed from the center of mass, reflect the partitioning of the total angular momentum between angular momenta of individual molecules and orbital angular momentum associated with their relative motion.

Crossed beam studies of several reactions of the type $M + RI \rightarrow R + MI$ are described, where M = K, Rb, Cs and R = CH_3, C_2H_5, etc. The results show that most of the energy of reaction goes into internal excitation of the products and that the angular distribution is quite anisotropic, with most of the MI recoiling backward (and R forward) with respect to the incoming K beam.

*Support received from the U. S. Atomic Energy Commission and the Alfred P. Sloan Foundation is gratefully acknowledged.

The molecular mechanics of chemical reactions can be studied most directly in crossed beam experiments. In recent years this prospect has captivated workers in several laboratories, and encouraging results have already been obtained.[1-7] Fortunately, there is a large class of reactions of alkali metals with halogen compounds which can be studied with almost rudimentary apparatus. The early flame studies of M. Polanyi[8] demonstrated that many of these reactions have very large cross sections, even larger than "hard-sphere" values; and the surface ionization studies of Langmuir provided a remarkably sensitive and specific detector for alkali atoms and their compounds.[9] Even for alkali reactions, in a typical crossed beam experiment the yield at the peak of the angular distribution corresponds to only a monolayer of product molecules per month.

The feasibility of such experiments was established in 1955 by the work of Taylor and Datz[2] on the reaction

$$K + HBr \rightarrow H + KBr \qquad (1)$$

Although the traditional tungsten surface ionization detector is about equally sensitive to K and KBr, Taylor and Datz found that a platinum alloy is much more effective for K than for KBr, and this enabled them to distinguish the reactive scattering from the large background of elastic scattering. The collision yield (ratio of total KBr detected to K scattered out of the parent beam) was found

to be 10^{-3} and an activation energy of 3 kcal/mole was estimated from the variation of the yield with beam temperatures. In 1960, Greene, Roberts, and Ross[3] reported a further study of reaction (1), with the important refinement of a mechanical rotor to select the K beam velocity. This has led, in recent work with Beck,[4] to detailed information about the dependence of the reaction probability on the initial relative translational energy and impact parameter of the reactants.

In the experiments at Berkeley,[5-7] we have been very fortunate to have the collaboration of G. H. Kwei, J. A. Norris, and J. L. Kinsey. Our first aim has been to study the distribution of velocity vectors of the products. This dictated the choice of a reaction which fulfilled certain kinematical requirements, to be outlined below. It was decided to try

$$K + CH_3I \rightarrow CH_3 + KI \qquad (2)$$

and analogous reactions. The restrictions imposed by the conservation laws make it possible to infer from the angular distribution of alkali halide in these reactions the final relative translational energy of the products as well as the directions in which they recoil away from the center of mass.

MECHANICS OF COLLISIONS

Energy and Linear Momentum

The conservation laws for energy and linear momentum provide geometrical relationships between the velocity vectors in the asymptotic initial and final states of a collision. Newtonian

mechanics is rigorously applicable here, as the same relationships hold in quantum mechanics.

The total energy available to the reaction products, to be partitioned between their final relative translational kinetic energy, E', and internal excitation, W' (rotational, vibrational, or electronic), is given by

$$E' + W' = E + W + \Delta D_o^\circ \ . \qquad (3)$$

The constant energy of the center of mass motion is omitted, E + W is the initial energy of the reactants, and ΔD_o° is the difference in dissociation energies of the products and reactants (measured from the zero-point vibrational levels).

An observer traveling with the constant velocity of the center of mass,

$$\underset{\sim}{c} = (m_1\underset{\sim}{v}_1 + m_2\underset{\sim}{v}_2)/m \ , \qquad (4)$$

would see the reactants approach with velocities inversely proportional to their masses and parallel to the relative velocity vector,

$$\underset{\sim}{v} = \underset{\sim}{v}_1 - \underset{\sim}{v}_2 \qquad (5)$$

since momentum conservation requires

$$\underset{\sim}{v}_1 - \underset{\sim}{c} = (m_2/m)\underset{\sim}{v} \qquad (6a)$$

$$\underset{\sim}{v}_2 - \underset{\sim}{c} = -(m_1/m)\underset{\sim}{v} \ . \qquad (6b)$$

The recoil velocities which carry the products away from the center of mass are correlated in the same way (see Fig. 1),

$$\underset{\sim}{v}_3 - \underset{\sim}{c} = (m_4/m)\underset{\sim}{v}' \qquad (7a)$$

$$\underset{\sim}{v}_4 - \underset{\sim}{c} = -(m_3/m)\underset{\sim}{v}' \ . \qquad (7b)$$

The final relative velocity vector,

$$\underset{\sim}{v}' = \underset{\sim}{v}_3 - \underset{\sim}{v}_4 \ , \qquad (8)$$

may take any direction in space, but energy conservation restricts its magnitude,

$$v' = (2E'/\mu')^{1/2} \ , \qquad (9)$$

which is determined by the reduced mass, μ', of the products and the final relative translational energy.

A convenient way to take into account the conservation laws in analyzing an observed laboratory distribution is to construct a "Newton diagram," as illustrated below in Figs. 6-9. For each of the accessible values of E', the spectrum of recoil vectors for product m_3 can range over a sphere of radius $(m_4/m)v'$ about the tip of $\underset{\sim}{c}$ (see Fig. 1b). The angle χ between $\underset{\sim}{v}$ and $\underset{\sim}{v}'$ describes the angular distribution, which has cylindrical symmetry about $\underset{\sim}{v}$, as shown later under Eq. (11). Corresponding vectors for product m_4 appear at the mirror image angle $\pi-\chi$ on a sphere of radius $(m_3/m)v'$. The Newton diagram thus displays the possible recoil spectrum of a product as a set of spheres, one for each value of E' up to the maximum allowed by Eq. (3).

To compare a theoretical model with experiment we must (i) derive from the model the density of recoil vectors per unit area over each sphere in the Newton diagram, (ii) project these distributions onto the laboratory coordinate system, and (iii) average over the initial velocity distributions in the incident beams.

For (1) we require the differential cross section per unit solid angle,

$$d\sigma/d\omega = I(\chi,E,E'), \qquad (10)$$

for which $I_3(\chi) = I_4(\pi-\chi)$. The partitioning of angular momentum in the reaction strongly influences the form of $I(\chi)$ and under certain conditions it will favor peaking along the direction of $\underset{\sim}{v}$, as indicated later.

When the reactant beams have comparable velocities, the transformation (ii) is much more complicated than that familiar in nuclear scattering,[10] and often introduces severe distortions in the laboratory "image" of $I(\chi)$. It is convenient to designate a product as "fast" or "slow" according as its recoil velocity (7) is greater or less than the center of mass velocity. As seen in Fig. 1b, the laboratory distribution of a fast product may range over 4π steradians, whereas that of a slow product is confined within a forward cone about $\underset{\sim}{c}$, regardless of the form of $I(\chi)$, and in general contributions from two values of χ are superimposed at each laboratory angle. Three cases may be identified in which the relations imposed by (ii) can be used to advantage by choosing reactions with suitable values of ΔD_o^o and mass ratios.

Case A: $|\underset{\sim}{v}_1 - \underset{\sim}{c}| \lesssim 0.1c$. All the KBr formed in reaction (1) is very slow, for example; even for the maximum possible value of E', it is confined within about 10° of $\underset{\sim}{c}$. This facilitates measurement of the total reaction cross section and its dependence on E. The variation of $I(\chi)$ with χ and E' has practically no effect on the laboratory distribution of product, which is essentially

determined just by the spread in $\underset{\sim}{c}$ arising from the velocity distributions of the reactants.[11,12]

Case B: $|\underset{\sim}{v}_i - \underset{\sim}{c}| \gtrsim 10c$. If a product is sufficiently fast over most of the range of E', its laboratory distribution will give the variation of $I(\chi)$ with χ directly, with negligible distortion from (ii). An example is the H atom produced in reaction (1). However, information about the dependence on E' cannot be obtained without a velocity analysis of the product. Also, for this case, important portions of the $I(\chi)$ distribution will often fall in regions obscured by elastic scattering or outside the range that can be scanned by the detectors.

Case C: $|\underset{\sim}{v}_i - \underset{\sim}{c}| \simeq c$. For a suitable intermediate case, the laboratory distribution will be strongly influenced by both χ and E'. This occurs for the KI formed in reaction (2), as shown in Fig. 2. Furthermore, as illustrated later, the main features of the dependence on χ and on E' can sometimes be untangled, without resorting to a velocity analysis of the product, by combining data from different experimental configurations. This is possible if the reactant beams have comparable velocities, as in reaction (2). The transformation relations of Fig. 2 are then drastically altered for out-of-plane scattering and for different angles of intersection of the reactant beams.

Angular Momentum

Conservation of angular momentum provides that

$$\underset{\sim}{L}' + \underset{\sim}{J}' = \underset{\sim}{L} + \underset{\sim}{J} , \qquad (11)$$

where $\underset{\sim}{L}$ and $\underset{\sim}{L}'$ denote the initial and final orbital angular momentum associated with the relative motion of the collision partners and

$$\underset{\sim}{J} = \underset{\sim}{J}_1 + \underset{\sim}{J}_2 \; ; \; \underset{\sim}{J}' = \underset{\sim}{J}_3 + \underset{\sim}{J}_4 \qquad (12)$$

are sums of the momenta of the individual reactant and product molecules. As indicated in Fig. 3a, the initial $\underset{\sim}{J}$ vectors are randomly oriented, whereas the $\underset{\sim}{L}$ vectors are perpendicular to the initial relative velocity $\underset{\sim}{v}$, with all azimuthal orientations of $\underset{\sim}{L}$ about $\underset{\sim}{v}$ equally likely. Therefore the total angular momentum $\underset{\sim}{L} + \underset{\sim}{J}$ always has a distribution with cylindrical symmetry about $\underset{\sim}{v}$ and (11) imposes this symmetry on the angular distribution of products.

There is another kinematical feature which, under certain conditions, can greatly enhance the correlation between the product distribution and the direction of $\underset{\sim}{v}$. Consider first the limiting case in which orbital angular momentum is conserved,

$$\underset{\sim}{L}' = \underset{\sim}{L} \; . \qquad (13)$$

(This holds precisely for elastic scattering in a central potential.) In this limit, the motion of both reactants and products is confined to a plane perpendicular to $\underset{\sim}{L}$. According to classical mechanics, the relation between the scattered intensity per unit angle in this plane, $d\sigma/d\chi$, and the differential cross section is

$$I(\chi) = (2\pi \sin \chi)^{-1} \, d\sigma/d\chi \; , \qquad (14)$$

where the first factor arises from integrating over the azimuthal orientations of $\underset{\sim}{L}$ about $\underset{\sim}{v}$. The situation is illustrated in Fig. 3b for the special case

$$d\sigma/d\chi = \text{constant}, \qquad (15)$$

which distributes the products uniformly over the azimuthal angles about $\underset{\sim}{L}$, like "water spraying off a spinning wheel." The complete angular distribution is obtained by rotating the diagram about $\underset{\sim}{v}$ so that the circle shown in Fig. 3b generates a sphere. Thus we see that the recoil vectors of the products will fan out around the equator and accumulate along the poles, as required by Eq. (14). Of course, Eq. (15) need not hold in general; the $1/\sin\chi$ factor in (14) will produce strong forward peaking whenever the planar distribution does not vanish at $\chi = 0°$, and backward peaking whenever it does not vanish at $\chi = 180°$. This has been called the "glory effect" in discussions of elastic scattering.[13] The peaking can be suppressed only when $d\sigma/d\chi$ vanishes sufficiently rapidly at the poles; for example, the angular distribution becomes isotropic only in the case of specular reflection of hard spheres (for which $d\sigma/d\chi$ is proportional to $\sin\chi$).

In reactive scattering Eq. (13) cannot be expected to hold. However, deviations from planar motion will be small when

$$\text{(a)}\ \ \underset{\sim}{L} \gg \underset{\sim}{J} \quad \text{and} \quad \text{(a')}\ \ \underset{\sim}{L}' \gg \underset{\sim}{J}', \qquad (16)$$

and the glory effect will then enter prominently. Averaging over the various orientations of $\underset{\sim}{J}$ and $\underset{\sim}{J}'$, which tilt the total angular momentum vector with respect to $\underset{\sim}{v}$ and $\underset{\sim}{v}'$, merely rounds off the peaking somewhat. As the conditions (16) are relaxed, the glory scattering persists to a surprising extent; calculations show it is still significant when $\underset{\sim}{J}$ and $\underset{\sim}{J}'$ carry over half of the angular momentum.[10] It fades away, of course, when either of the

inequalities in (16) is reversed; thus, if $\underset{\sim}{L} \ll \underset{\sim}{J}$, the distribution of directions of the total angular momentum vector becomes nearly isotropic and hence no longer endows the products with a "memory" of the direction of $\underset{\sim}{v}$.

In the analysis of $I(\chi)$ it is therefore often appropriate to separate three factors: the partitioning of the total angular momentum (i) between $\underset{\sim}{L}$ and $\underset{\sim}{J}$ and (ii) between $\underset{\sim}{L}'$ and $\underset{\sim}{J}'$; and (iii) the distribution $d\sigma/d\chi$, which now refers to a plane perpendicular to the total angular momentum vector.

A rough estimate of (i) may be made by comparing the distribution of J, as given by a rotational partition function, with that of L, derived from the classical relation

$$L = \mu v b \qquad (17)$$

by compounding the distributions of initial relative velocity and impact parameter. Reaction is assumed to occur for all values of b up to a maximum, which is approximated by equating πb^2 to the total reaction cross section. For most chemical reactions, including (1) and (2), it is found that L is substantially larger than J, and accordingly (i) does not inhibit the glory effect. For such reactions, factors (ii) and (iii) decide whether the angular distribution of products will show pronounced anisotropy. Several reaction models have been examined which suggest that in many cases (ii) is likely to be the dominant factor.[10] For example, the simplest model to treat assumes a "sticky" collision complex which lives long enough to make Eq. (15) hold; that is, longer than the relaxation time required for the decay of phase relations

associated with formation of the complex. A characteristic feature of this model is that the angular distribution of products must be symmetrical about $\chi = 90°$. If it is also assumed that (ii) is fixed by the population of rotational states of the complex (regarded as in thermal equilibrium at the saddle-point of a potential energy surface), the angular distribution is readily calculated in terms of the moments of inertia and rotational temperature of the complex and the total available angular momentum inferred from Eqs. (17) and (11). For reactions (1) and (2), any reasonable assignment of these parameters predicts $L' >> J'$, and hence strong scattering both forward and backward along $\underset{\sim}{y}$.

In this brief survey, only a few aspects of the connection between reaction mechanism and angular distribution could be mentioned. Others are developed in a more detailed, quantum mechanical treatment.[10] Like the present classical discussion, much of this is adapted from the theory of nuclear reactions.[14] Classical theory is usually qualitatively correct for chemical reactions, which typically involve very large angular momenta; however, the infinite peaking at the poles predicted by Eq. (14) and other sharp edges of the classical approximation are smoothly rounded off in the quantum treatment.

APPARATUS AND EXPERIMENTAL CONDITIONS

As shown in Fig. 1, the beams are formed by thermal effusion from ovens mounted on a turntable which is rotated to sweep the angular distribution past the detector. Vertical adjustment of the detector position allows the scattering to be measured out of

the plane (angle ϕ, accessible from 0° to ± 40°) as well as in the plane of the incident beams (angle θ, accessible over -30° to 150° from the alkali beam). The detector is similar to that described by Taylor and Datz[2,15]; after the initial aging, the tungsten filament is usually operated at 1900°K, the platinum alloy filament at 1800°K. The two chambers of the alkali oven are separately heated. The temperature of the beam, which issues from the upper chamber, can thus be varied about three hundred degrees without affecting the vapor pressure, which is fixed (at about 0.1 mm Hg) by the temperature of the molten alkali in the lower chamber. The gas oven is connected to an external barostat by a supply tube (not shown in Fig. 1) which passes through the support column in the rotating lid. Cold shields and collimating slits hide both ovens from the scattering center, and a cold shield also surrounds the detector. The entire scattering chamber is enclosed in a copper box attached to a large liquid nitrogen trap. For condensable reactants this provides a very high pumping speed (estimated as 200,000 liters/sec) and although this apparatus lacks the customary differential pumping of the beam sources, the background pressure remains at 10^{-7} mm Hg during runs.

For measurements of in plane scattering "tall beams" are used; the oven slits are ordinarily made 0.025 cm wide by 1 cm high and the collimating slits adjusted to give beams between 0.05 and 0.20 cm wide at the scattering center. For measurements of out of plane scattering the detector filaments (both 0.005 cm in diameter) and the beams are made "flat"; the beams are then only 0.025 cm high and 0.2 to 0.4 cm wide. Increasing the narrow dimension of the oven

slits would not lead to increased beam intensity as the pressure within the oven would have to be decreased proportionately to satisfy the condition for effusive flow. The distance from the scattering center to the alkali oven is 11 cm; to the gas oven slit, 1.7 cm; and to the detector usually 10 cm in the tall configuration and 4 cm in the flat configuration.

Auxiliary experiments showed the detector filaments to be unaffected by alkyl iodides except for a slight increase in noise. It was also confirmed that the tungsten filament is about equally sensitive to M and MI, whereas the platinum alloy was found to be about 50 times more efficient for M than for MI (in disagreement with data in the literature[15]). Test runs made with nonreactive materials as the cross beam, such as n-heptane, showed that the relative detection efficiencies of the tungsten and the platinum alloy filaments for M remained constant over the range of intensities of interest for the study of reactive scattering. However, the readings often failed to match in the region close to the M beam (within $\pm$ 25°) where the intensity of elastic scattering rises very steeply; the discrepancies here may be due mainly to insufficiently precise interchanging of the filament positions. These runs also indicated that any "diffusion-pump" action of the crossed beam[16] was negligibly small.

In the K + CH_3I experiments, the concentration of K within the volume defined by the intersection of the beams is about 10^{10} atoms/cc, equivalent to a pressure of 10^{-6} mm, and that of CH_3I is about 100-fold greater. About 10^{14} K atoms/sec enter the reaction volume, of which roughly 0.1% react to form KI while about 10% undergo

elastic scattering. In beam experiments elastic scattering always predominates, since quite weak interactions will deflect a molecule from the beam. The total cross section for beam scattering[17] of K + CH_3I is about 1400 A^2 and implies that encounters in which the K and CH_3I pass at a distance of 20 Å count as collisions; at this distance the intermolecular potential energy amounts to only 0.3 cal/mole. The steady-state concentration of KI in the reaction volume is roughly 10^7 molecules/cc, the pressure 10^{-9} mm. At the peak of the KI distribution about 10^7 molecules/sec arrive at the detector.

SUMMARY OF RESULTS

An example of the data obtained[5] for reaction (2) is shown in Fig. 5. The KI distributions are normalized so that the area under the curves gives the collision yield, which is 5 x 10^{-4} and corresponds to a reaction cross section of about 7 A^2. Variation of the K beam temperature over a range of 250°K gives practically no change in the yield and indicates the activation energy is less than 0.3 kcal/mole.

The Newton diagram of Fig. 6, constructed from Eqs. (3) and (6)-(9), compares the observed angular distribution with that allowed by the conservation laws. In Eq. (5), ΔD_o^o = 22 kcal/mole; the thermal distribution of initial kinetic energy is peaked at E = 1.3 kcal/mole; and the CH_3I is mostly in the ground vibrational state with a rotational distribution peaked near W = 0.6 kcal/mole. It is seen that the broad peak observed near 83° in the laboratory corresponds to scattering in which an observer stationed at the

center of mass would see KI recoil backward (and CH_3 forward) with respect to the incoming K beam. The displacement of almost 35° from the direction of $\underset{\sim}{c}$ shows that the main contributions must have $E' \gtrsim 1$ kcal/mole. Also, as illustrated by the vector labeled $\underset{\sim}{a}$, reactions producing large values of E' can contribute to the peak only if the recoil velocity vector deviates considerably from the direction of the initial relative velocity $\underset{\sim}{v}$ (see also Fig. 2). Since the recoil vectors must have cylindrical symmetry about $\underset{\sim}{v}$, such contributions can be studied directly by measurement of the out-of-plane scattering. As the KI is found to be peaked about the plane of the incident beams, we may conclude that scattering close to the direction of $\underset{\sim}{v}$ with small values of E' is predominant. Experiments at various angles of intersection of the beams confirm this. It is found that the in-plane KI peak shifts to 68° and to 129° for intersection angles of 60° and 135°, respectively, in agreement with predictions derived by redrawing the Newton diagram for these intersection angles (see Fig. 9). In order to account for the observations, 50% of the KI recoil vectors must lie within the doubly shaded region in fig. 6 and 90% within the singly shaded region. These regions were derived by a calculation which combined the in-plane and out-of-plane data and included the velocity distributions in the reactant beams. Also shown in Fig. 6 is the estimate of the most probable CH_3 recoil velocity implied by eqn. (7) and this analysis of the KI distribution. Velocity selection[18] is essential if the resolution is to be improved, as illustrated by the dashed curve in Fig. 5b. This was calculated by averaging over the initial distribution of $\underset{\sim}{v}$ vectors, assuming that all of the KI

recoiled directly backwards along $\underset{\sim}{v}$ (that is, $\chi = 0°$) with internal excitation $W' \cong 21$ kcal/mole (corresponding to $E' - E = 1.6$ kcal/mole).

From the results for reaction (2), we can predict what to expect for the angular distributions in other M + RX reactions, if we assume the products will show a similar peaking about the direction of $\underset{\sim}{v}$ and high internal excitation. The results found for the reactions of Rb[6] and Cs atoms with CH_3I, shown in Fig. 7 and 8, have peaks within a few degrees of the predictions. The activation energy is again found to be negligibly small for these reactions. The reactions of K atoms with ethyl, i-propyl, n-propyl, and n-butyl iodides have also been studied. Under conditions similar to those of Fig. 5, all these reactions have KI peaks in the neighborhood of 90°. This indicates, according to Eq. (7b), that the average E' decreases as the mass of the R group is increased. There is no noticeable effect from "steric interference" as the R group becomes larger; the collision yield remains about the same as for the CH_3I reaction.

A question of particular interest, but not yet entirely settled, is the possible presence of "forward" scattering of the alkali halide, corresponding to recoil angles near $\chi = 180°$. As can be seen from Fig. 2, for large E' most of this would appear in the region $-30° < \theta_{KI} < 30°$, which is hidden by elastic scattering from the parent K beam (see Fig. 5). There is evidence that the recoil distribution is not symmetrical about 90°, however.[7] The dashed curves in Fig. 9 (calculated as before with $E' - E = 1.6$ kcal/mole, and equal intensity at $\chi = 0°$ and 180°) indicate that a prominent

shoulder should have been observed in the region $30° < \theta_{KI} < 50°$, if a forward peak complementary to the observed backward peak were present.

DISCUSSION

The rather primitive experiments described here may suffice to illustrate both the present limitations of the beam method and some of its potentialities. Because the products are observed immediately after the collision in which they are formed, even the qualitative results already obtained pose interesting new questions for the theory of chemical kinetics.

For all the reactions studied, the average relative translational energy of the products inferred from the angular distributions is comparable to that of the reactants. Thus roughly 90% of the energy of reaction appears as internal excitation. The present results offer no information about the partitioning of this energy among various degrees of freedom, but presumably it is largely present as vibration of the newly-formed bond. In contrast, spectroscopic studies have in several cases provided a detailed picture of both the vibrational and rotational disequilibrium of a reaction product, but not yet under conditions that permit conclusions about the initial excitation.[19,20] The spectroscopic results and theoretical models concerned with the vibrational excitation of products have recently been reviewed by Basco and Norrish[19] and by J.C. Polanyi.[21]

The observed asymmetric peaking of the angular distribution along the direction of the initial relative velocity vector implies a reaction mechanism with specific properties. The lack of symmetry about $\chi = 90°$ shows that the decomposition of the collision complex cannot be regarded as independent of its manner of formation (as in the compound nucleus model of nuclear reactions[14]); the initial phase relations are not entirely "forgotten." The suppression of $\chi = 180°$ scattering (thus far established only for $E' \gtrsim 10$ kcal/mole) must be attributed to anisotropy in the planar cross section, $d\sigma/d\chi$. However, the prominence of scattering near $\chi = 0°$ could arise either from the form of $d\sigma/d\chi$ or, if the final orbital angular momentum is large enough, from the glory effect. (This is, incidentally, opposite to the directional preference of the "stripping" collision model for nuclear reactions.[14]) Scattering near $\chi = 0°$ evidently corresponds to a "hard" collision rather than to a "grazing" one, as the M atom, the R group, and the center of mass of M and I must all reverse direction. It would seem plausible to assume that $d\sigma/d\chi$ is not restricted to be strongly peaked at $\chi = 0°$, and to interpret the observed peaking as mainly due to a gloriously large final orbital angular momentum. According to Eq. (16), the reaction then takes place more or less in a plane, and the picture suggested by the asymmetry is that the complex decomposes before it can rotate through a half-turn. As the rotational velocities estimated from Eq. (17) are very high, roughly half of the complexes would have to decompose within about 5×10^{-13} seconds, a time not much longer than a vibrational period.

Footnotes

[1]Bull and Moon, Faraday Soc. Discussions, 1954, 17, 54.

[2]Taylor and Datz, J. Chem. Physics, 1955, 23, 1711.

[3]Greene, Roberts, and Ross, J. Chem. Physics, 1960, 32, 940.

[4]Beck, Greene, and Ross, Second International Conference on Electronic and Atomic Collisions (Benjamin, New York, 1961), p. 94.

[5]Herschbach, Kwei, and Norris, J. Chem. Physics, 1961, 34, 1842.

[6]Kinsey and Kwei, Bull. Am. Physic. Soc., 1961, 6, 152.

[7]Norris, Bull. Am. Physic. Soc., 1961, 6, 339.

[8]Polanyi, Atomic Reactions (Williams and Norgate, London, 1932).

[9]Langmuir and Kingdon, Proc. Roy. Soc., 1923, 21, 380; see also Fraser, Molecular Rays (Cambridge, 1931), p. 43.

[10]Herschbach, J. Chem. Physics (to be published).

[11]Herschbach, J. Chem. Physics, 1960, 33, 1870.

[12]Datz, Herschbach, and Taylor, J. Chem. Physics, 1961, 35, 1549.

[13]Ford and Wheeler, Ann. Physics, 1959, 7, 287.

[14]See, for example, I. Halpern, Nuclear Fission, Ann. Rev. Nuc. Sci., 1959, 9, 245; V. F. Weisskopf, Physica, 1956, 22, 955; Butler, Nuclear Stripping Reactions (Wiley, New York, 1957).

[15]Datz and Taylor, J. Chem. Physics, 1956, 25, 395.

[16]Nutt and Biddlestone, Nature, 1961, 191, 798; Trans. Faraday Soc. (in press, 1962).

[17]Rothe and Bernstein, J. Chem. Physics, 1959, 31, 1619.

[18]Kwei, work in progress.

[19]Basco and Norrish, Can. J. Chem., 1960, 38, 1769.

[20]Cashion and Polanyi, J. Chem. Physics, 1961, 35, 600.

[21]Polanyi, J. Chem. Physics, 1959, 31, 1338.

Captions for Figures

Fig. 1 Relations among the velocity vectors of (a) reactants and (b) products. Masses are numbered such that $m_1 \leq m_2$ and $m_3 \leq m_4$.

Fig. 2 Transformation relating angle and energy in center of mass and laboratory coordinate systems, for the in-plane scattering corresponding to Fig. 6. Contours of constant χ are shown by solid curves, contours of constant E' by dashed curves.

Fig. 3 (a) Orientation of initial angular momentum vectors. (b) Distribution of recoil vectors for "sticky collision" model discussed in text.

Fig. 4 Sketch of apparatus. Cold shields, collimating slits, shutters to interrupt the beams, and other details omitted.

Fig. 5 (a) Parent K beam of 5×10^{-8} amps attenuated 7% by crossed CH_3I beam. Readings on Pt detector (solid circles) normalized to W (open circles) at parent beam peak. (b) KI distributions; circles derived from (a), triangles from a replicate experiment (several months later). Area under curves gives collision yield.

Fig. 6 Newton diagram corresponding to most probable velocities of reactants in Fig. 5.

Fig. 7 Results for Rb reaction.

Fig. 8 Results for Cs reaction.

Fig. 9 Test for possible presence of "forward peaking."

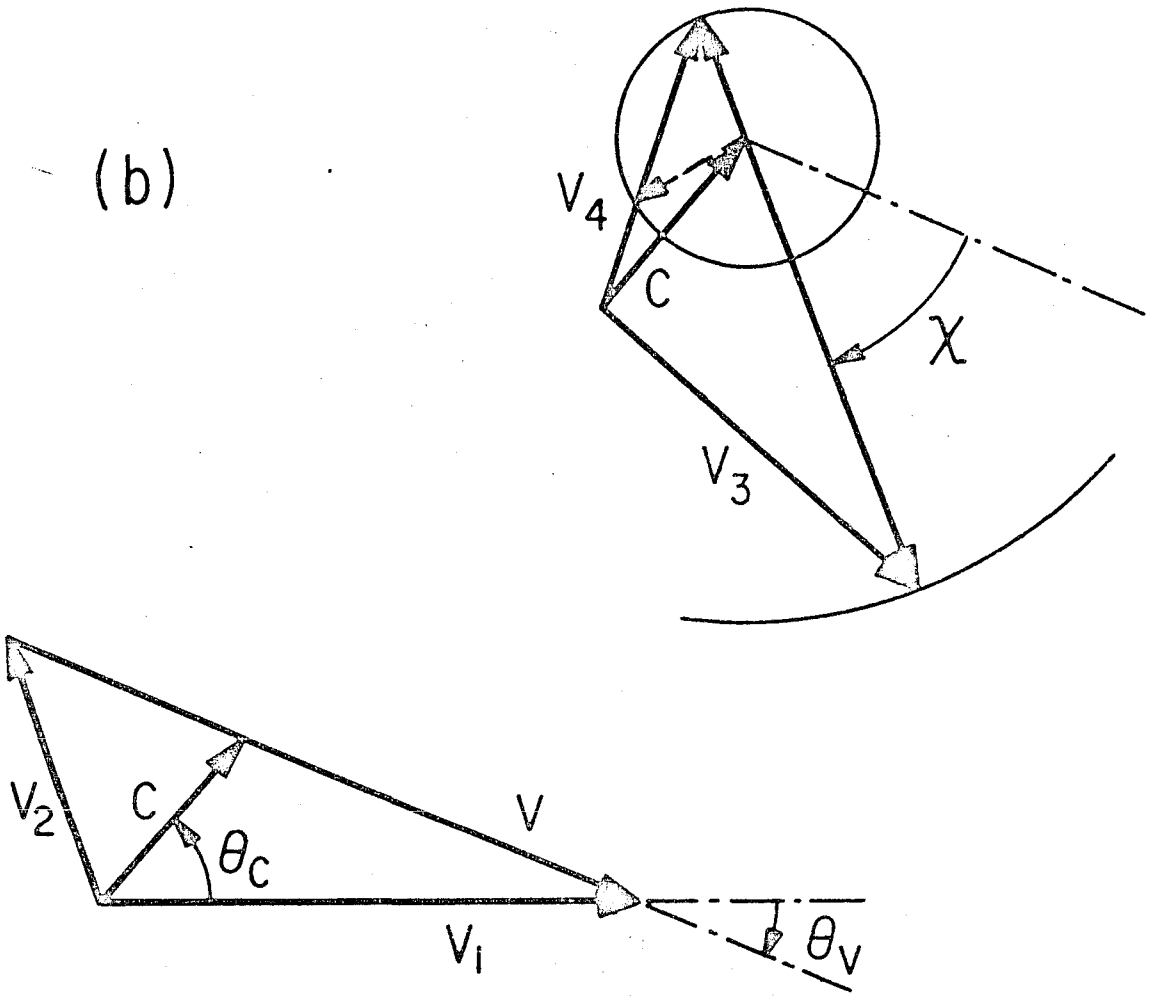

Fig. 1

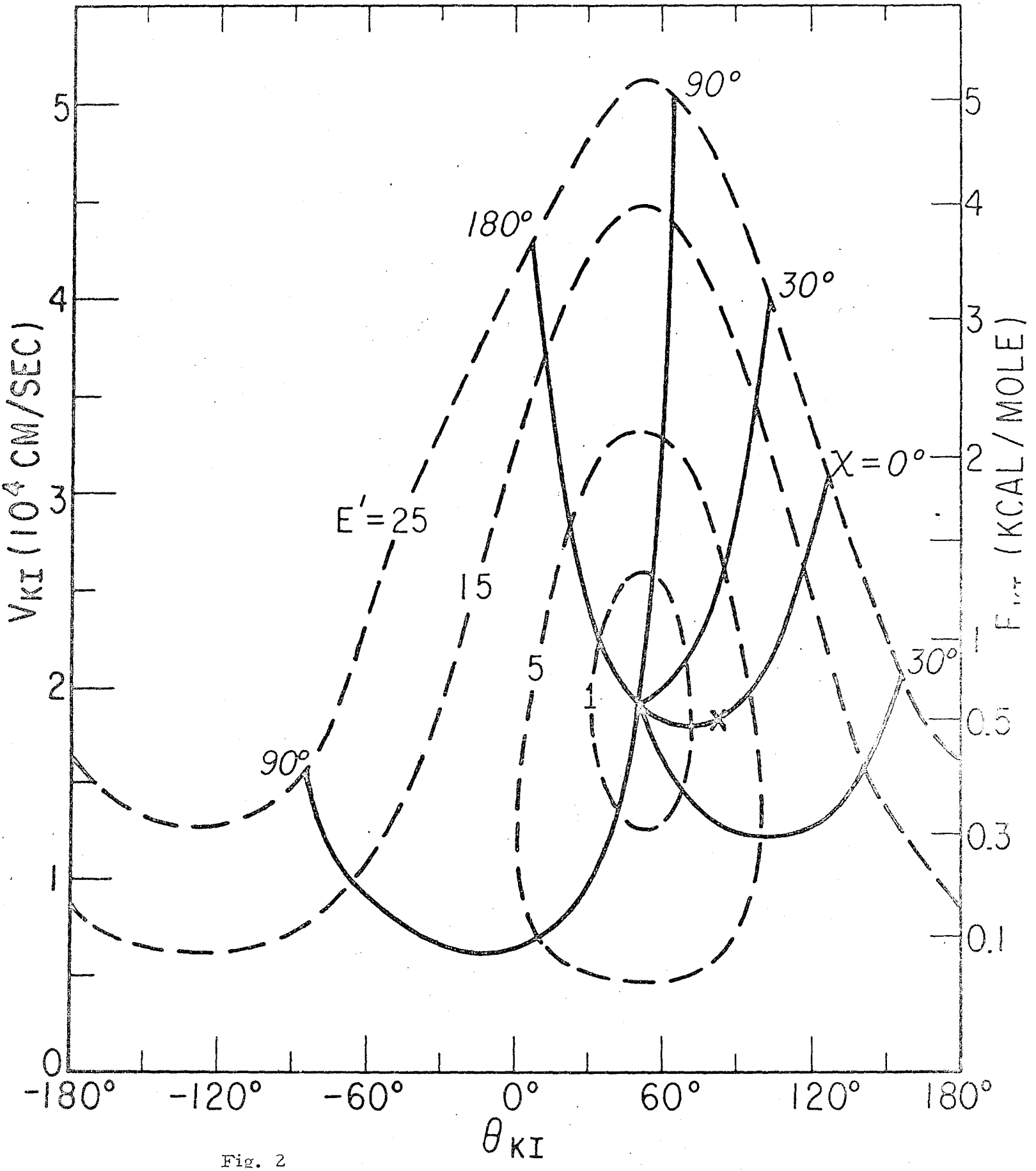
90°
180°
30°
X = 0°
E' = 25
15
5
1
90°
30°
V_{KI} (10^4 CM/SEC)
F_{KI} (KCAL/MOLE)
θ_{KI}
-180°
-120°
-60°
0°
60°
120°
180°
0
1
2
3
4
5
0.1
0.3
0.5
1
2
3
4
5

Fig. 2

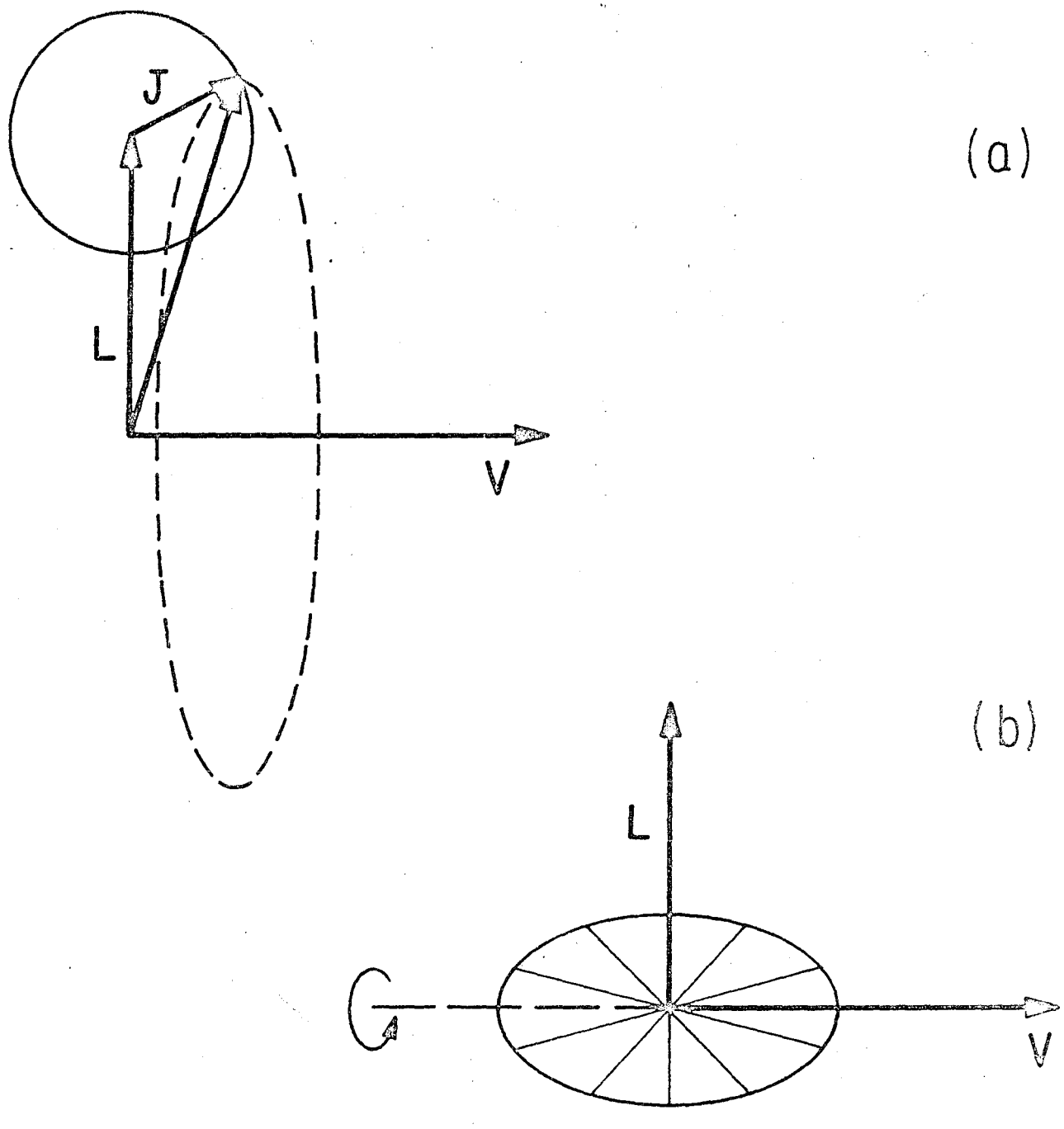

Fig. 3

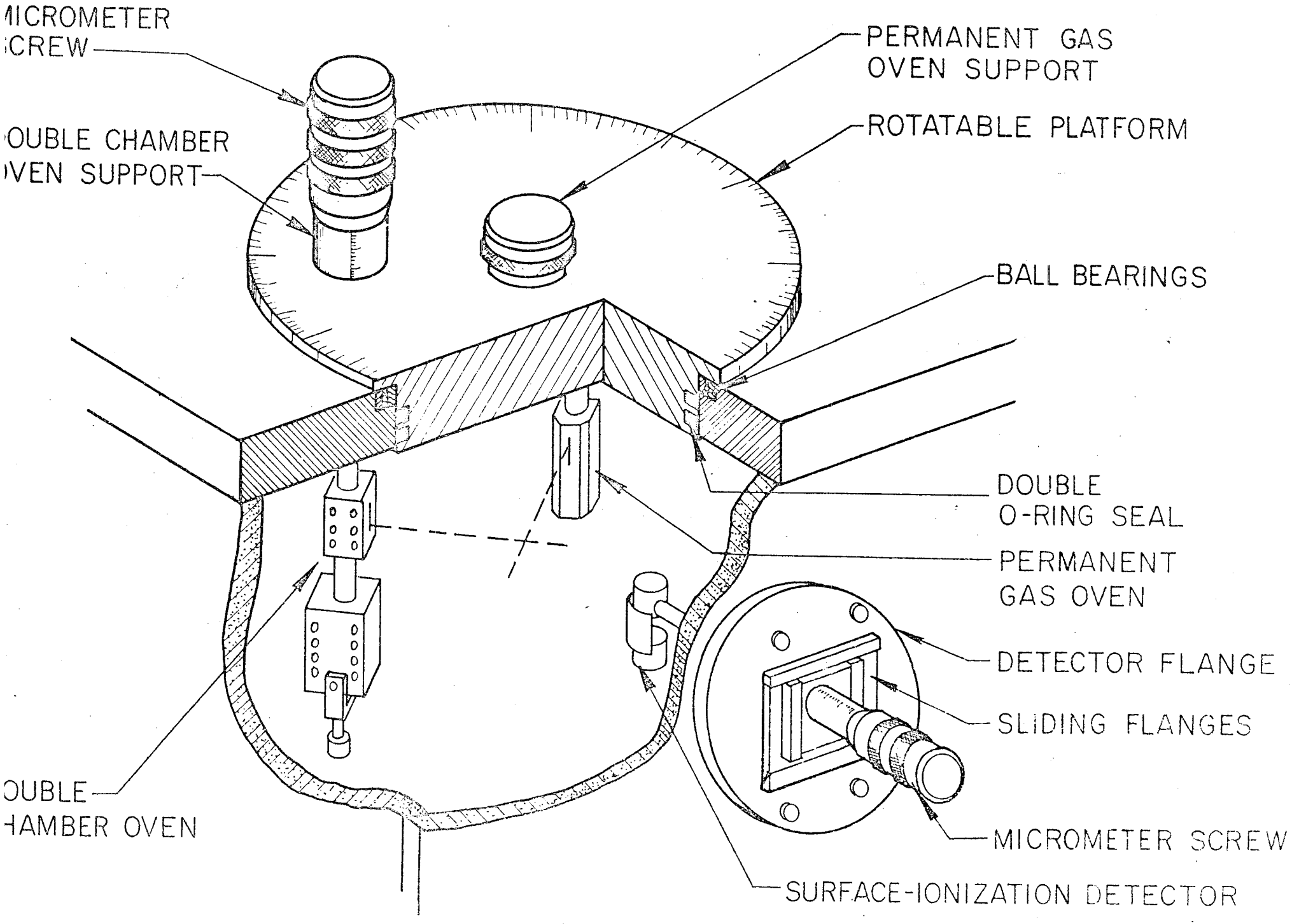
MICROMETER SCREW
PERMANENT GAS OVEN SUPPORT
DOUBLE CHAMBER OVEN SUPPORT
ROTATABLE PLATFORM
BALL BEARINGS
DOUBLE O-RING SEAL
PERMANENT GAS OVEN
DETECTOR FLANGE
SLIDING FLANGES
DOUBLE CHAMBER OVEN
MICROMETER SCREW
SURFACE-IONIZATION DETECTOR

Fig. 4

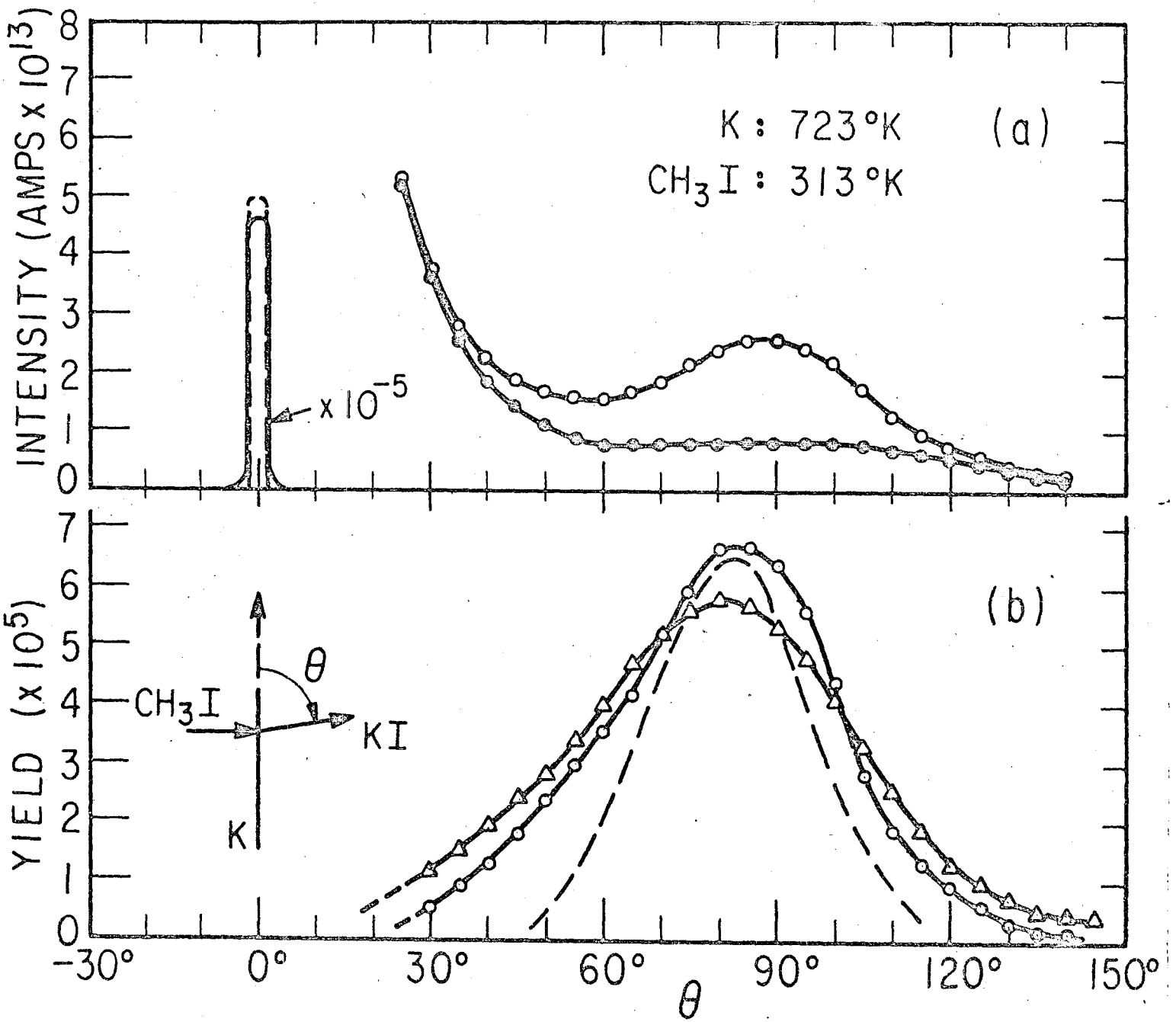
INTENSITY (AMPS x 10^13)
K : 723°K
CH3I : 313°K
(a)
x 10^-5
YIELD (x 10^5)
(b)
θ
CH3I
KI
K
-30°
0°
30°
60°
90°
120°
150°
θ

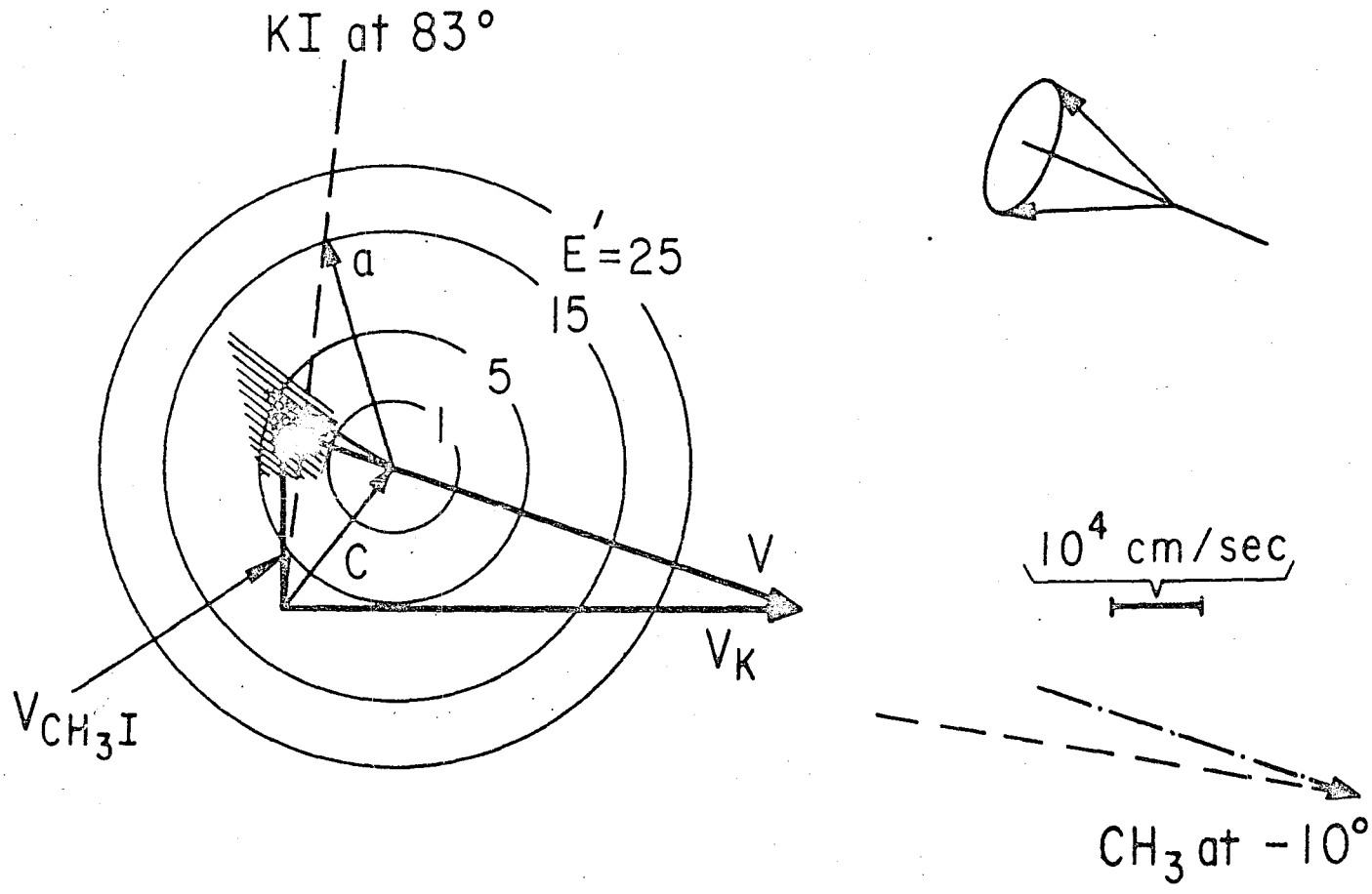

Fig. 6

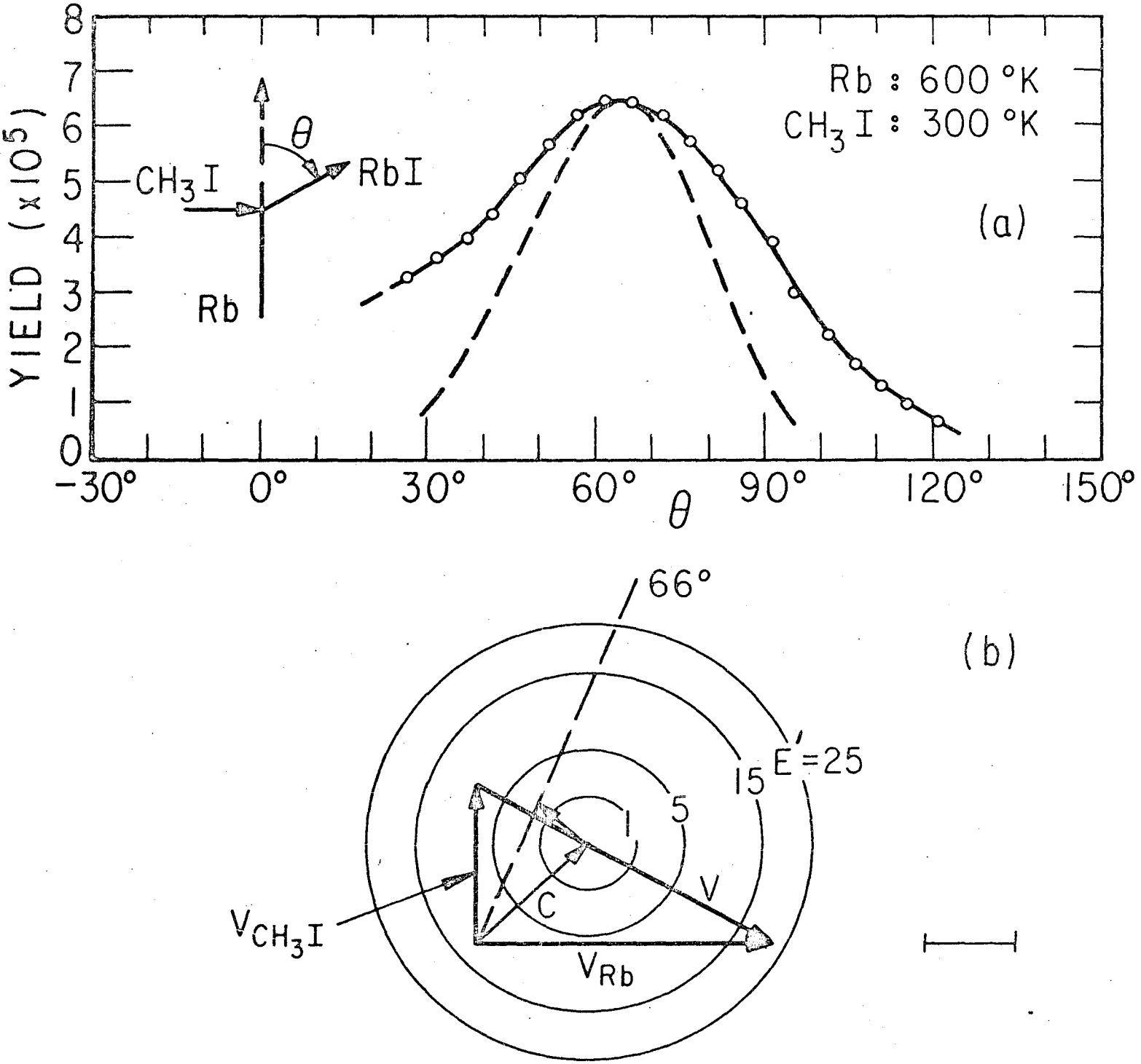
YIELD (x10⁵)
8
7
6
5
4
3
2
1
0
-30°
0°
30°
60°
90°
120°
150°
θ
Rb : 600 °K
CH₃I : 300 °K
(a)
θ
CH₃I
RbI
Rb
66°
(b)
E′=25
15
5
1
V
C
V_CH₃I
V_Rb

Fig. 7

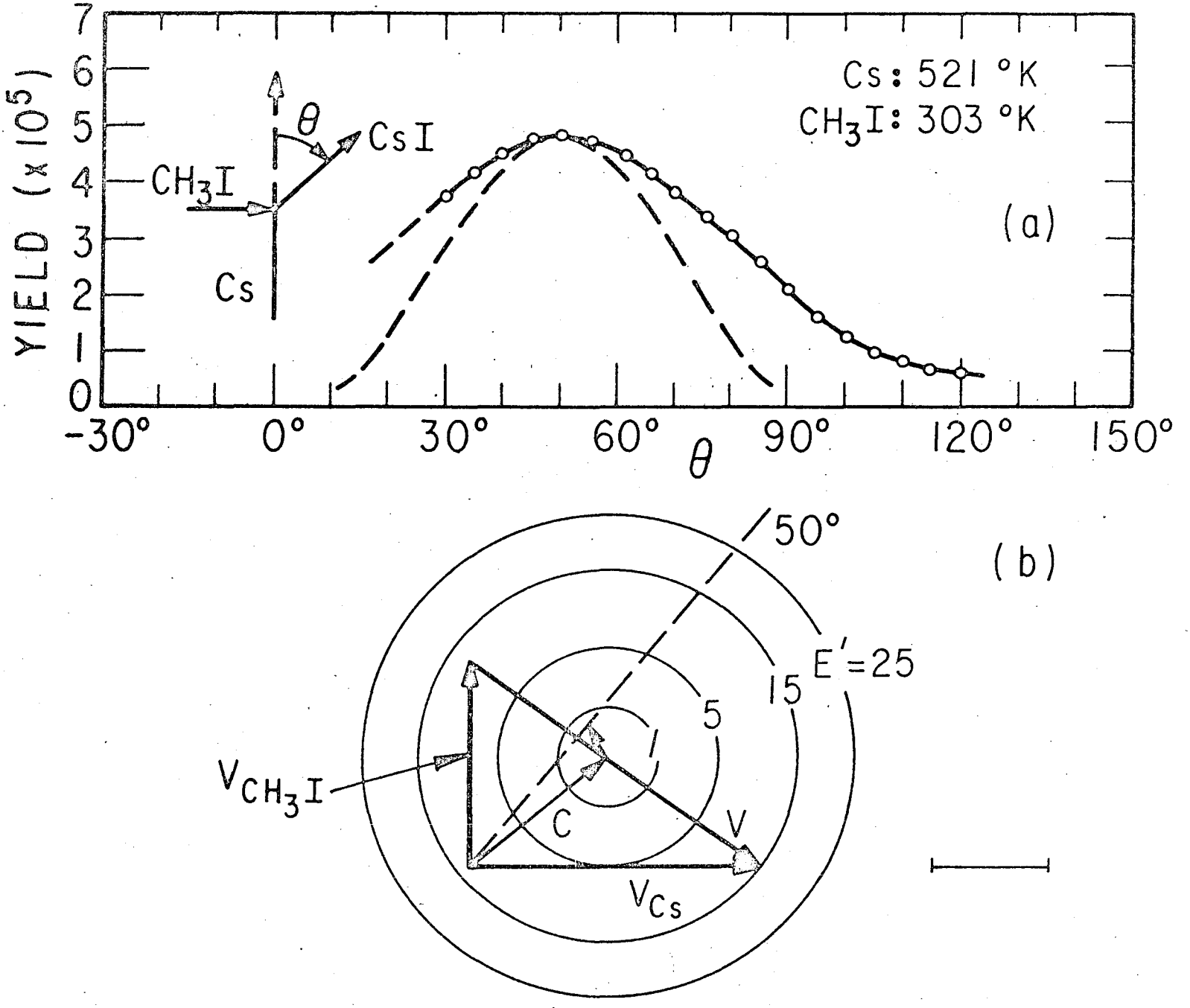
YIELD (x 10^5)
7
6
5
4
3
2
1
0
-30°
0°
30°
60°
90°
120°
150°
θ
Cs: 521 °K
CH3I: 303 °K
(a)
θ
CsI
CH3I
Cs
50°
(b)
E'=25
15
5
VCH3I
C
V
VCs

Fig. 8

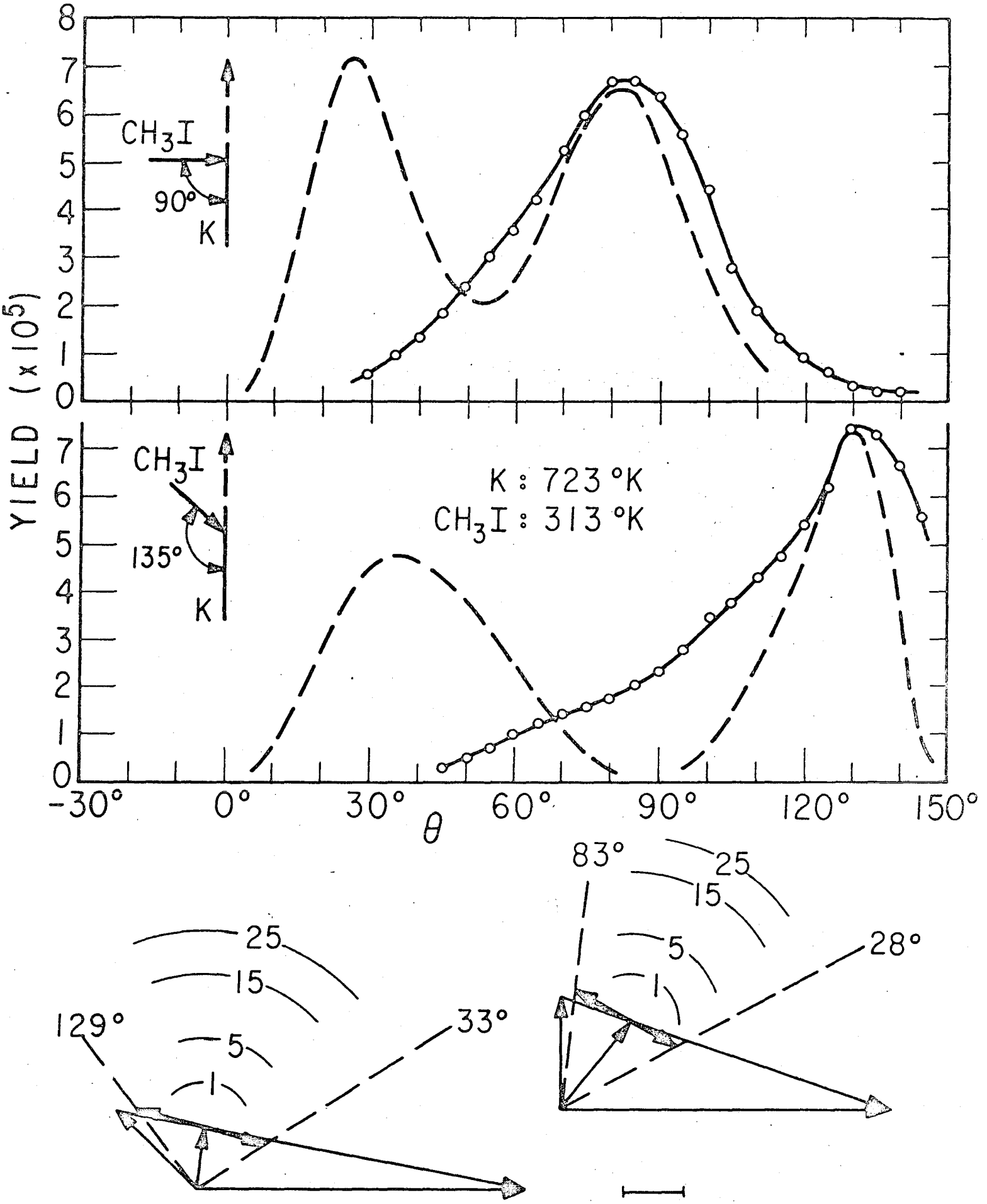
YIELD (x10^5)
CH3I
90°
K
CH3I
135°
K
K : 723 °K
CH3I : 313 °K
θ
-30°
0°
30°
60°
90°
120°
150°
129°
25
15
5
1
33°
83°
25
15
5
1
28°

Fig. 9